



Waterproof molecular monolayers stabilize 2D materials

Cong Su^{a,b,1}, Zongyou Yin^{c,1,2}, Qing-Bo Yan^{a,d,1}, Zegao Wang^{e,f}, Hongtao Lin^{g,h}, Lei Sunⁱ, Wenshuo Xu^j, Tetsuya Yamada^k, Xiang Ji^b, Nobuyuki Zettsu^k, Katsuya Teshima^k, Jamie H. Warnerⁱ, Mircea Dincăⁱ, Juejun Hu^g, Mingdong Dong^e, Gang Su^l, Jing Kong^{b,m}, and Ju Li^{a,g,2}

^aDepartment of Nuclear Science and Engineering, Massachusetts Institute of Technology, Cambridge, MA 02139; ^bResearch Lab of Electronics, Massachusetts Institute of Technology, Cambridge, MA 02139; ^cResearch School of Chemistry, The Australian National University, ACT 2601, Australia; ^dCollege of Materials Science and Opto-Electronic Technology, University of Chinese Academy of Sciences, 100049 Beijing, China; ^eInterdisciplinary Nanoscience Center, Aarhus University, 8000 Aarhus, Denmark; ^fCollege of Materials Science and Engineering, Sichuan University, 610065 Chengdu, China; ^gDepartment of Materials Science and Engineering, Massachusetts Institute of Technology, Cambridge, MA 02139; ^hCollege of Information Science & Electronic Engineering, Zhejiang University, 310027 Hangzhou, China; ⁱDepartment of Chemistry, Massachusetts Institute of Technology, Cambridge, MA 02139; ^jDepartment of Materials, University of Oxford, OX1 3PH, United Kingdom; ^kCenter for Energy and Environmental Science, Shinshu University, 380-8553 Nagano, Japan; ^lSchool of Physical Science, University of Chinese Academy of Sciences, 100049 Beijing, China; and ^mDepartment of Electrical Engineering and Computer Science, Massachusetts Institute of Technology, Cambridge, MA 02139

Edited by Michael L. Klein, Temple University, Philadelphia, PA, and approved September 11, 2019 (received for review June 4, 2019)

Two-dimensional van der Waals materials have rich and unique functional properties, but many are susceptible to corrosion under ambient conditions. Here we show that linear alkylamines $n\text{-C}_m\text{H}_{2m+1}\text{NH}_2$, with $m = 4$ through 11, are highly effective in protecting the optoelectronic properties of these materials, such as black phosphorus (BP) and transition-metal dichalcogenides (TMDs: WS_2 , $1\text{T}'\text{-MoTe}_2$, WTe_2 , WSe_2 , TaS_2 , and NbSe_2). As a representative example, n -hexylamine ($m = 6$) can be applied in the form of thin molecular monolayers on BP flakes with less than 2-nm thickness and can prolong BP's lifetime from a few hours to several weeks and even months in ambient environments. Characterizations combined with our theoretical analysis show that the thin monolayers selectively sift out water molecules, forming a drying layer to achieve the passivation of the protected 2D materials. The monolayer coating is also stable in air, H_2 annealing, and organic solvents, but can be removed by certain organic acids.

molecular monolayer stabilizer | multilayer 2D materials | anticorrosion

Passivation of materials in air and water is foundational to our civilization (1). When we consider the robust ultrathin passivation of 2D materials (2–7), it should be even more essential because 1) the thickness of passivation layer on 3D materials like Si, Al, Cr, etc. stays 2 to 5 nm over a very long time, which is an insignificant fraction of the remaining unreacted bulk material. However, one cannot say this for thin 2D materials with their total thickness likely comparable to the native oxide passivation layers. Thus, the atomistic details of passivation matter even more here. 2) An ultrathin, electronically insulating layer provides opportunity to engineer extremely thin vertical heterostructures, akin to the SiO_2/Si gate in metal-oxide-semiconductor field-effect transistors. For these reasons, it is becoming increasingly critical to facilely passivate layered materials such as transition-metal dichalcogenides (TMDs), black phosphorus (BP), silicene, stanine (8–12), etc., which are susceptible to corrosion under ambient conditions with air, water, or even small amounts of acidic or basic contaminants (9, 10, 13–19).

Several passivation strategies have been developed for these layered materials including covering by more robust 2D materials such as graphene (20) and hexagonal boron nitride (21). However, many previous strategies suffer from processability issues and other drawbacks: Metal-oxide coatings are prone to cracking (14, 22); polymers [e.g., poly(methyl methacrylate) (PMMA), polystyrene, Parylene, and perylene-3,4,9,10-tetracarboxylic dianhydride] are readily attacked by organic solvents and offer limited durability (19, 23–26); self-assembled monolayers with silane-terminated octadecyltrichlorosilane are highly toxic (27). Here, we discovered a one-pot scalable process for passivating a large variety of 2D van

der Waals materials. It involves coating a nanometer-thick monolayer of linear alkylamines onto the surface of 2D materials, which greatly increases the lifetime of these materials in ambient environments with moisture and can sustain even harsh aqueous and thermal conditions. First-principles simulations suggest that the alkylamine coating significantly slows down the permeation of O_2 , which reacts with the 2D layered material to form an ultrathin oxide passivation layer, and completely blocks H_2O molecules and shuts down the cycles of oxidation–dissolution, leading to the extended lifetime for many different classes of 2D crystals.

Since BP is the most vulnerable to corrosion among the 2D van der Waals (vdW) materials studied in this work and creates the most challenges for processing, it is used here as an illustrative example of the alkylamine coating. As a representative example of linear alkylamines $n\text{-C}_m\text{H}_{2m+1}\text{NH}_2$, n -hexylamine ($m = 6$) coating onto BP is systematically investigated both theoretically and experimentally in its corrosion inhibition mechanism and behaviors.

Results

The coating process is divided into 2 steps: 1) The sample together with silicon substrate is put in the liquid n -hexylamine for 20 min under 130 °C. This step creates coating on sample, but minor cracks might exist. 2) To fix the cracks, the sample is then immersed in hexylamine vapor for another 20 min at 130 °C and then annealed in argon for 30 min under 200 °C after the surface

Significance

A family of strong yet removable 1- to 2-nm-thick ultrathin monolayer is developed as a corrosion inhibitor for 2-dimensional materials that significantly prolong lifetime while protecting optoelectronic properties in both ambient and harsh chemical or thermal environments. This method is low in toxicity and can be applied to arbitrary substrate with no size limit.

Author contributions: C.S., Z.Y., and J.L. designed research; C.S., Z.Y., Q.-B.Y., Z.W., H.L., W.X., T.Y., and X.J. performed research; C.S., Z.Y., L.S., N.Z., K.T., J.H.W., M. Dincă, J.H., M. Dong, G.S., J.K., and J.L. analyzed data; N.Z., K.T., J.H.W., M. Dincă, J.H., M. Dong, G.S., J.K., and J.L. supervised the project; and C.S., Z.Y., and J.L. wrote the paper.

Competing interest statement: US Patent under International Application PCT/US2018/025174 has been filed for technique related to this work.

This article is a PNAS Direct Submission.

Published under the PNAS license.

¹C.S., Z.Y., and Q.-B.Y. contributed equally to this work.

²To whom correspondence may be addressed. Email: Zongyou.yin@anu.edu.au or liju@mit.edu.

This article contains supporting information online at www.pnas.org/lookup/suppl/doi:10.1073/pnas.1909500116/-DCSupplemental.

is cleaned by hexane. The hexane cannot remove the hexylamine coating but only the surface contamination, as shown later. More detailed coating procedures are presented in *SI Appendix, Fig. S1* (28–40). The optimization of coating parameters of *n*-hexylamine onto BP is shown in *SI Appendix, Table S1*.

Once mechanically exfoliated, the bare BP flakes are highly reactive and chemically unstable. After keeping a 3-nm-thick BP flake in ambient air (humidity $\sim 35\%$) for 2 d (the thickness is estimated using the method from ref. 9), only vague traces remain (Fig. 1A), even when care is taken to prevent light exposure, known to accelerate the damage. As shown in Fig. 1A, the 3 characteristic Raman peaks of BP at 361 cm^{-1} (A_g^1), 438 cm^{-1} (B_{2g}), and 466 cm^{-1} (A_g^2) completely disappear after 2 d. The degradation of BP is further expedited when exposed to light, in line with previous reports (9) which showed that the lifetime of BP (defined as the time needed for the Raman intensity to drop to e^{-1} of its original) is $\tau \sim 1\text{ h}$ when a 2.8-nm-thick sample is exposed to a photon flux of $1.8 \times 10^3\text{ W/cm}^2$, and $\tau \sim 10\text{ min}$ when exposed to a photon flux of $1.7 \times 10^4\text{ W/cm}^2$.

In contrast, *n*-hexylamine protected BP (HA-BP hereafter), which is kept side-by-side with the unprotected one, exhibits robust BP characteristics for a much-extended period. The difference in optical contrast for HA-BP between 0 and 111 d is essentially indiscernible (Fig. 1B); 31% of the intensity of A_g^2 was retained after 111 d. The photon fluence seen by HA-BP during Raman measurements in 111 d is equivalent to light

exposure of $1.0 \times 10^5\text{ W/cm}^2$ for $\sim 2\text{ h}$ in total. Since such photon exposure is already known to be substantial to cause the degradation of bare BP (ref. 9), we conclude that the lifetime of HA-BP can be extended even further if the sample has not been exposed to the laser beam of the Raman characterization.

The coating process involves the proton transfer of the hydroxylated BP to the $-\text{NH}_2$ group of *n*-hexylamine based on the evidence below. First-principles simulations suggest that *n*-hexylamine forms a molecular monolayer as shown in Fig. 2A. The top layer of the BP surface is rapidly oxidized from the oxygen dissolved in liquid hexylamine, forming P–OH, P–O $^-$, or P=O surface groups. Experimental evidence supports a model where the acidic P–OH groups on the BP surface and the terminal $-\text{NH}_2$ groups of alkylamines undergo a Brønsted–Lowry acid–base reaction to form a layer of alkylammonium salts that coat the BP surface through a strong electrostatic interaction with the deprotonated P–O $^-$ surface sites. Confirmation that the neutral $-\text{NH}_2$ group in *n*-hexylamine becomes charged (i.e., $-\text{NH}_3^+$) came from X-ray photoelectron spectroscopy (XPS): Comparing the N 1s peaks between HA-BP, dodecylamine ($\text{C}_{12}\text{H}_{25}\text{NH}_2$, R– NH_2), and methylammonium chloride ($\text{CH}_3\text{NH}_3\text{Cl}$, R– NH_3^+) reveals that HA-BP and R– NH_3^+ have the same binding energy, which is blueshifted by 2.4 eV from that of R– NH_2 (Fig. 2B). Contact-angle measurements also show that the surface of BP becomes more hydrophobic after HA coating (*SI Appendix, Fig. S2*), confirming that the HA coating is indeed terminated by alkyl chains, not by amine/ammonium groups.

Inspection by atomic force microscopy (AFM) of the height profile of the same 2D flake before and after coating revealed that the *n*-hexylamine coating is around 1.5 nm thick (Fig. 2C), which is consistent with the theoretical chain length of *n*-hexylamine (41). This demonstrates that the deposition of *n*-hexylamine molecules is self-limiting. Polar organic solvents including acetone, ethanol, or isopropanol, as well as nonpolar solvents like hexane, cannot remove the *n*-hexylamine coating, indicating that the interaction between *n*-hexylamine and BP is strong enough to sustain solvent attack. We also note that *n*-hexane does not impart any corrosion protection, attesting that the amine group is key for this function and that the alkyl chain itself cannot bind strongly on BP.

We employed first-principles calculations to investigate the transfer of protons when *n*-hexylamine approaches P–OH (Fig. 2D), formed by reacting with the water from the *n*-hexylamine coating solution. Among various structural possibilities after systematic study, with results shown in *SI Appendix, Figs. S3–S6*, the most likely reaction pathway agrees with the scenario (P–O $^-$ – NH_3^+ – C_6H_{13}) proposed above and yields a bonding energy of 0.97 eV, which is 3 to 4 \times stronger than the pure vdW interaction [$\sim 0.33\text{ eV}$ between *n*-hexylamine and pure BP, $\sim 0.22\text{ eV}$ between amines and graphene (42)]. The electronic density distribution shows that the H atom shares its orbital much more with N atom than with O atom (Fig. 2D, *Inset*), and Bader charge analysis indicates that *n*-hexylammonium ($\text{C}_6\text{H}_{13}\text{NH}_3^+$) carries a net charge of $+0.89e$, and to compensate, the rest has $-0.89e$.

In Fig. 2E, the migration energy barrier of H_2O penetrating through *n*-hexylamine is calculated to be 1.4 eV and O_2 1.0 eV, when *n*-hexylamine covers BP in the densest possible packing structure (hereafter defined as 100% coverage, shown in *SI Appendix, Figs. S8 and S9*); when the coverage drops to 66.7%, the migration energy barrier reduces to 0.2 eV for H_2O permeation and no barrier (0 eV) for O_2 . When the HA coverage further decreases to 50% or 25%, the migration of both H_2O and O_2 through the HA layer toward the surface of BP is barrierless. Combining this theoretical analysis with the time-evolution XPS data on phosphorus oxide concentration (Fig. 2F and G), where the oxidization speed of phosphorus after *n*-hexylamine coating is significantly reduced by 32 \times at the beginning of oxidation (fitting method and definition of time constant can be found in

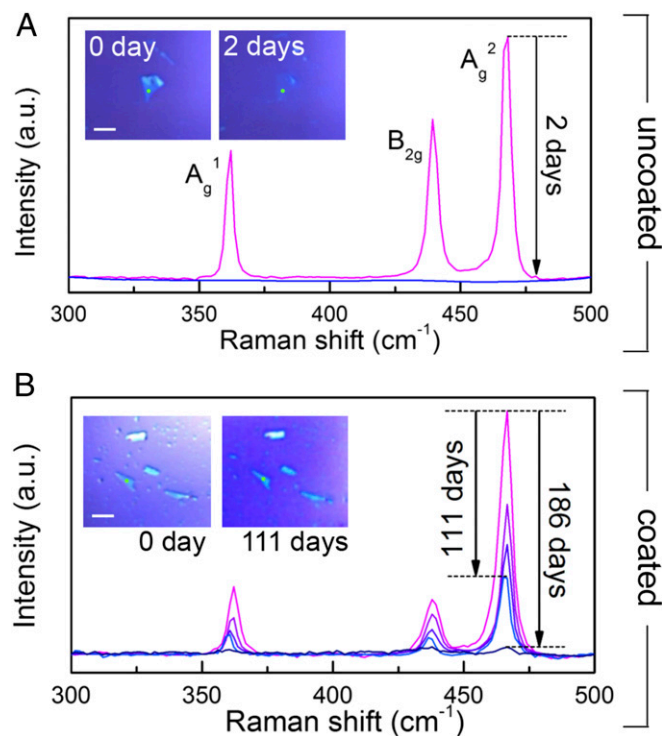


Fig. 1. Comparison of BP flakes with and without *n*-hexylamine coating. (A) The Raman spectra at $\lambda = 532\text{ nm}$ of the bare BP flake. (*Insets*) Optical images of the exfoliated BP flake on SiO_2/Si wafer before aging (on 0 d), and after 2-d aging in ambient conditions where only the blurry marks of original flake could be identified. (B) The corresponding Raman spectra of the *n*-hexylamine-coated sample on the 0, 13, 41, 111, and 186 d. (*Insets*) Optical images of *n*-hexylamine-coated BP flakes on SiO_2/Si before aging (on 0 d), and after 111-d aging under the same ambient conditions. (*Insets*) Green dots are laser spot positions for repeated spectra acquisition. All samples are dried for 30 min at 120°C in air right after being prepared. All Raman spectra shown above have been renormalized and calibrated to Si (reference) peak intensity. (Scale bars, $5\ \mu\text{m}$.)

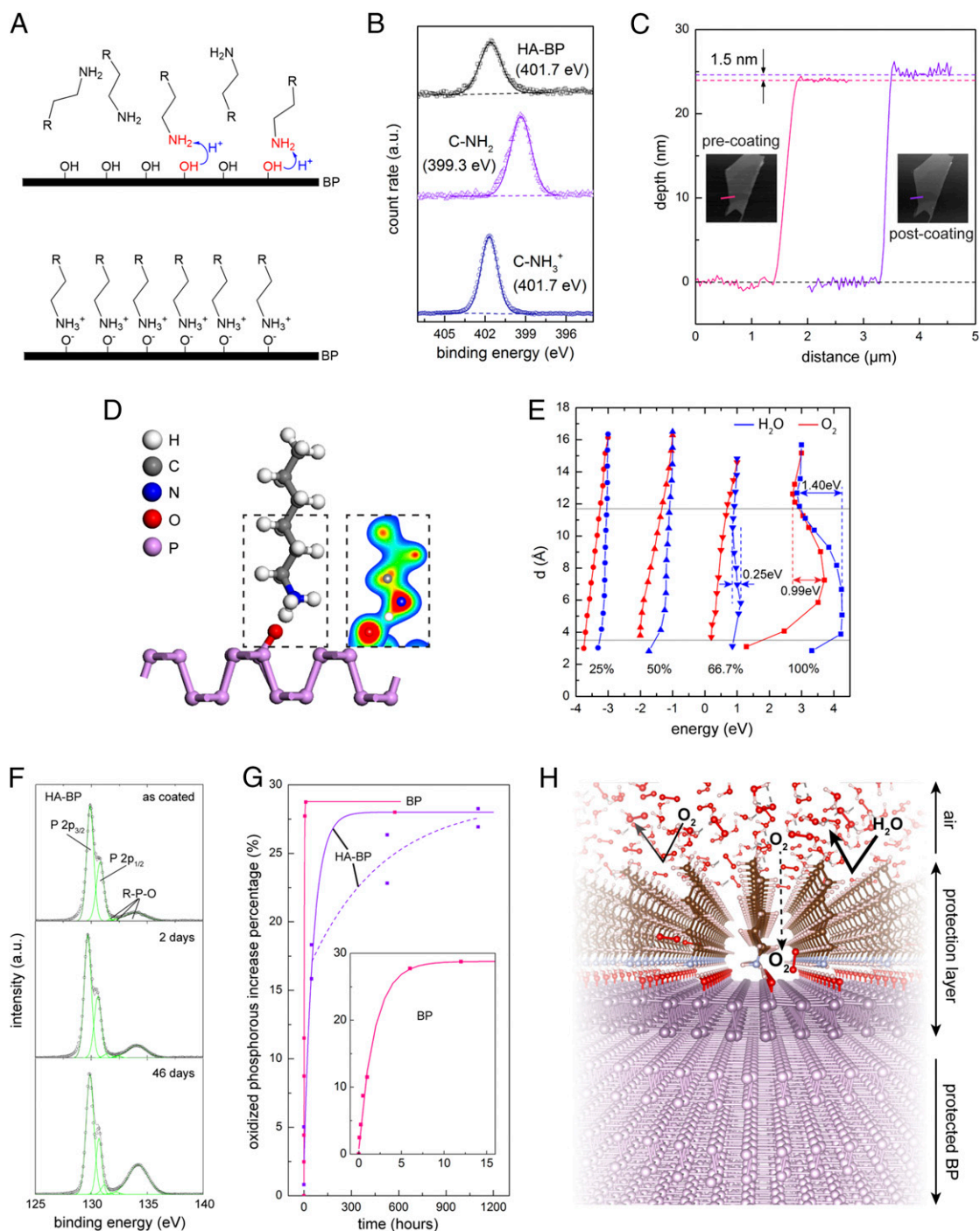


Fig. 2. The mechanism of *n*-hexylamine coating on BP. (A) Proton transfer takes place during the coating process (*Upper*) and the *n*-hexylamine monolayer is formed on BP after the coating process is done (*Lower*). R- in the diagram refers to C_6H_{13} when representing hexylamine. (B) XPS spectra of nitrogen 1s peaks on HA-BP, dodecylamine (C-NH₂), and CH₃NH₃Cl (C-NH₃⁺), proving that the amino group of *n*-hexylamine coated on BP is in ionic state -NH₃⁺. (C) The AFM data revealing the thickness of a BP flake with 24 nm before coating (pink line) and the thickness increment after hexylamine coating (violet line). (D) The schematic structure of *n*-hexylamine adsorbed on BP, where red-, blue-, gray-, purple-, and white-colored balls represent oxygen, nitrogen, carbon, phosphorus, and hydrogen, respectively. (*Inset*) the contour map of valence electron density on the plane containing O, N atoms and the H atom between them, which corresponds to the part marked by rectangle dashed line. (E) The energy profile of H₂O and O₂ molecules when penetrating through the hexylamine molecule layer. The y axis is the distance between the bottom atom of H₂O or O₂ and the surface of BP, denoted as *d*. Blue and red curves represent H₂O and O₂ penetration processes, respectively. The 4 groups of curves represent different coverages of 25, 50, 66.7, and 100% (detailed coverage definition illustrated in *SI Appendix, Fig. S7*), as marked. The horizontal gray lines are the locations of the top and the bottom of hexylamine molecules. (F) The P 2p peaks and oxidized phosphorus species (R-P-O) of XPS curves on HA-BP measured as coated, after 2 d, and after 46 d. (G) The phosphorus oxide concentration as a function of time between *n*-hexylamine-coated (violet triangles) and uncoated BP samples (pink squares). (*Inset*) A blow-up of the uncoated sample data between 0 and 15 h. Both datasets are fitted with exponential curves. The pink and violet solid lines are fittings of the scattered data pointing to the uncoated and HA-coated samples, respectively. Note that the oxidation of HA-BP is a significant slowdown starting from 100 h, so a second curve fitting is marked (dashed violet line). (H) Schematic illustration of the structure of BP after coating by *n*-hexylamine. The first layer of BP is oxidized and forms a part of protective layer together with the *n*-hexylamine coating. The surface protective layer (hexylammonium + first-layer oxidized BP) protects the rest of BP underneath.

SI Appendix), we deduce the coverage density of *n*-hexylamine on BP must be more than the defined 66.7% coverage on the surface of BP.

With these conclusions, a schematic illustration of the molecular monolayer can be shown in Fig. 2H. The top oxidized BP layer of PO_x together with the coated *n*-hexylamine monolayer forms a dense protection layer for the BP underneath. It lowers the penetration speed of O₂ molecule significantly and blocks the H₂O molecule almost completely under room temperature, thus stabilizing the surface passivation layer (the oxidized BP at the top).

The anticorrosion effect conferred by organic monolayer is not limited to *n*-hexylamine. Indeed, other linear alkylamines *n*-C_{*m*}H_{2*m*+1}NH₂ with *m* = 4 through 11, including *n*-butylamine (*n*-C₄H₉NH₂), *n*-pentylamine (*n*-C₅H₁₁NH₂), *n*-octylamine (*n*-C₈H₁₇NH₂), *n*-decylamine (*n*-C₁₀H₂₁NH₂), and *n*-undecylamine (*n*-C₁₁H₂₃NH₂), all consistently displayed similar anticorrosion effects in ambient air. Their coatings onto BP for anticorrosion demonstration are presented in *SI Appendix*, Table S2, and the growth parameters for coating all these alkylamines with different carbon chain lengths are summarized in *SI Appendix*, Table S3.

To demonstrate the passivation efficacy for actual optoelectronic devices in ambient and aggressive environments, we fabricated 2 BP-flakes-based photodetectors. As a direct bandgap semiconductor, with its *E*_{gap} continuously tunable from ~2 eV (single layer) to 0.3 eV (bulk) (43) by varying the number of layers, BP stands out as a promising material for photonic devices from near-infrared to midinfrared. The layout of the uncoated BP detector with a channel length and width of ~3 and ~5 μm, respectively, between the Ti/Au electrodes is shown in Fig. 3A. The thickness of the BP here is 74 nm (*SI Appendix*, Fig. S10). The *n*-hexylamine-coated BP photodetector is shown in Fig. 3B, with comparable channel dimension and a BP thickness of 55 nm (*SI Appendix*, Fig. S10). Note here, the photocurrent for bare BP device is significantly lower than the protected one due to the fast degradation of BP in air during sample loading and contacting electrical probes. The photocurrent and current density as a function of input optical power under zero voltage bias (Fig. 3A and B, uncoated and coated respectively) was measured in ambient air with a 1,550-nm laser. The coated BP can sustain annealing in H₂ environment under 250 °C for 1 h, proved by H₂O₂ etching experiment. Both devices exhibited increased photocurrent with input power before etching (black lines labeled with preetching in these plots). After dipping the devices in H₂O₂ for 5 s and drying them subsequently, obvious degradation was observed under optical microscope on the uncoated BP device (Fig. 3A, Upper-Right Inset), while little change was found on the coated one (Fig. 3B, Upper-Right Inset). As evidenced by the photoelectric signal, corrosion caused severe damage to the uncoated optoelectronic device, with the photocurrent dropping to 0. In contrast, the *n*-hexylamine-coated photodetector device maintained 78.6% of its original photocurrent based on the photocurrent values of 28.7 μA at postetching and 36.5 μA at preetching under photoexcitation with the same input power of 3 mW. The slight drop of performance likely originates from defects in the coating layer within the boundaries between the electrode metal and the BP flake, and also likely originates from the residue of PMMA during the deposition of electrodes that blocks the spreading of hexylamine.

Such monolayer protection is effective not only for BP, but also for other layered 2D materials. Here, to accelerate corrosion tests for *n*-hexylamine-coated 2D materials, we used harsh aqueous H₂O₂ or KMnO₄ solutions as etchants. In Table 1, we take the optical microscopy images during the corrosion exposure for each 2D material, including BP, WS₂, WSe₂, 1T'-MoTe₂, WTe₂, TaS₂, and NbSe₂. It should be noted that exfoliated BP, 1T'-MoTe₂, WTe₂, NbSe₂ and chemical vapor deposition (CVD)-grown single-layer WS₂ are known to be particularly susceptible to

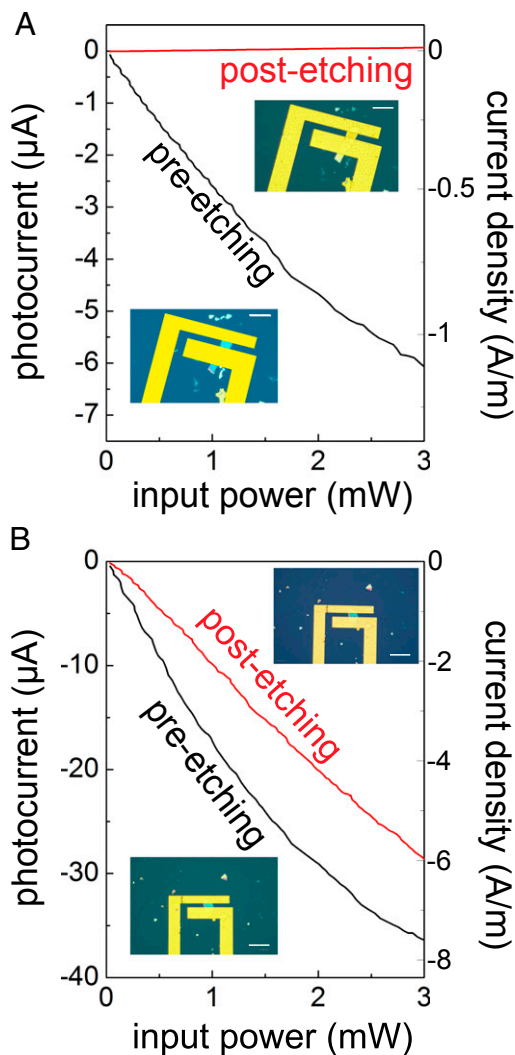


Fig. 3. Photodetectors and etching test. (A) Photocurrent and current density as a function of input optical power under zero bias voltage. (Insets) The optical images of uncoated BP devices before (Bottom Left) and after etching (Top Right) by an aqueous solution of 30 wt % H₂O₂ for 5 s. (B) *n*-hexylamine-coated-device counterparts of A. (Scale bars, 10 μm.)

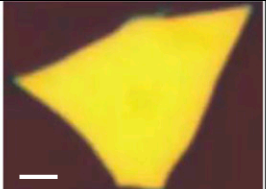
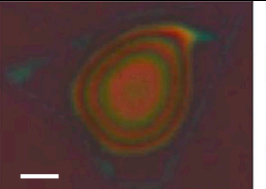
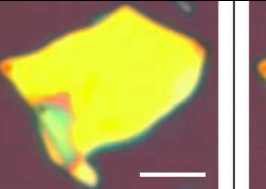
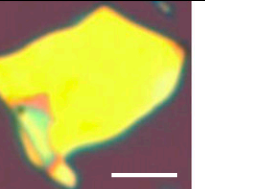
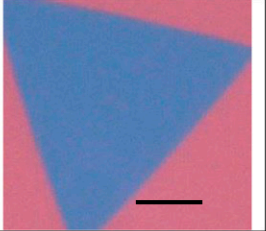
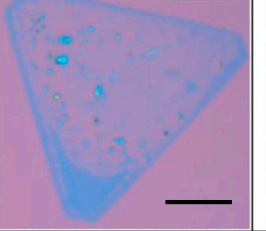
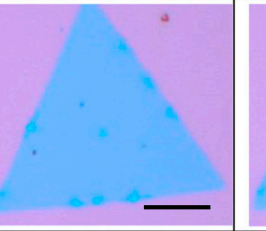
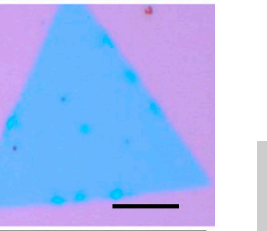
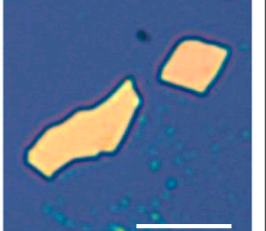
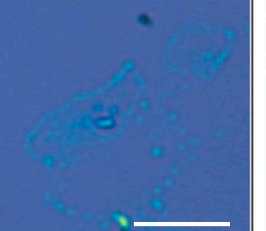
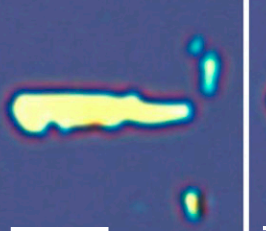
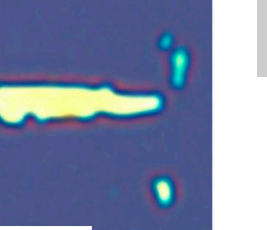
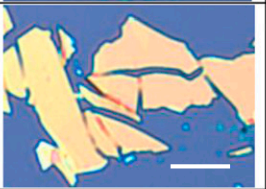
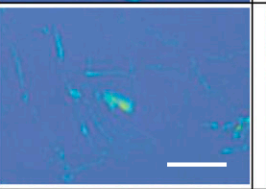
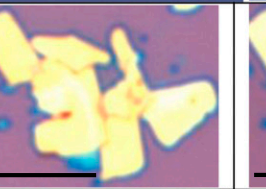
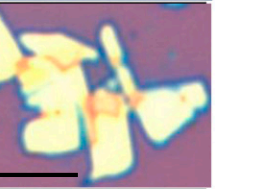
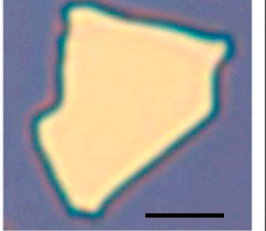
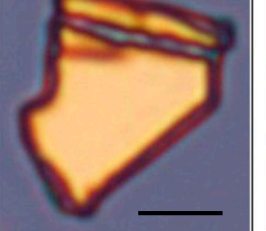
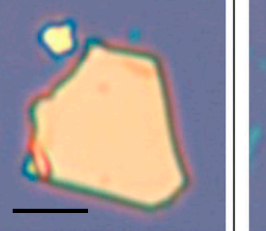
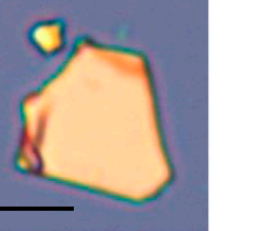
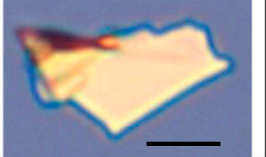
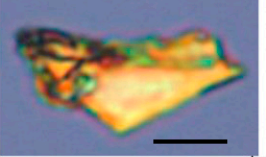
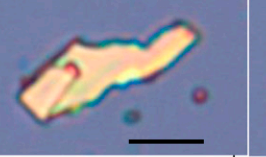
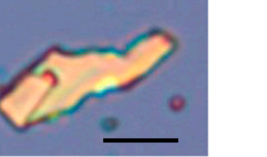


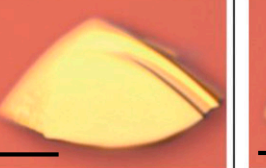

ambient corrosion and are readily attacked by solutions of H₂O₂. WSe₂ and TaS₂ are less vulnerable and require stronger oxidants for corrosion. *n*-hexylamine is proved to be effective in protecting these layered materials based on the comparison in optical image between uncoated and coated 2D materials after their exposure to the same etchants. A movie of the corrosion retardation for BP is presented as [Movie S1](#).

Despite the fact that *n*-hexylamine is sturdy under various environments, it is still removable by certain organic acids. Presumably, the organic-media-supported protons can penetrate the hydrophobic alkyl layer and protonate the ionized surface P-O⁻ groups, disrupting their electrostatic interaction with the alkylammonium cations. This removing protocol is effective both for the amine coating on BP and TMDs, without affecting the passivation oxidized layer and the materials underneath (*SI Appendix*, section 5).

Discussion

Amines with low water solubility have long been known as efficient and reliable corrosion inhibitors for steels (41, 44). It is found here that they also serve as an effective coating for 2D

Table 1. Protection of various 2D materials with *n*-hexylamine coatings

material / etchant with etching time	bare		coated	
	before exposure	after exposure	before exposure	after exposure
BP (exfoliated) / 20sec in H ₂ O ₂ (30 wt. % in H ₂ O)				
WS₂ (CVD, monolayer) / 5sec in H ₂ O ₂ (30 wt. % in H ₂ O)				
1T'-MoTe₂ (exfoliated) / 10sec in H ₂ O ₂ (30 wt. % in H ₂ O)				
WTe₂ (exfoliated) / 30sec in H ₂ O ₂ (30 wt. % in H ₂ O)				
WSe₂ (exfoliated) / 1min in KMnO ₄ (0.02mol/L in H ₂ O)				
TaS₂ (exfoliated) / 1min in KMnO ₄ (0.01mol/L in H ₂ O)				
NbSe₂ (exfoliated) / 20sec in H ₂ O ₂ (30 wt. % in H ₂ O)				

BP, WS₂, 1T'-MoTe₂, WTe₂, WSe₂, TaS₂, and NbSe₂ were coated with *n*-hexylamine and dipped inside etchants of H₂O₂ or KMnO₄ solution (depending on the respective material reactivity) as an accelerated lifetime test. The uncoated counterparts were processed in parallel with the coated parts under identical etching conditions. (Scale bars, 10 μm.)

layered materials, by blocking water for the native thin-oxide layer growing at the interface between the 2D material and the alkylamine coating. The photooxidation of bare BP starts with the synergetic effect of oxygen, water, and light, where phosphorus transformed to a layer of acidic phosphorus species. The thin layer of acid then coarsens into a droplet, leaving a fresh phosphorus surface in contact with ambient air, and the oxidation process starts once again (45). *n*-hexylamine monolayer lowers the permeability of oxygen and strongly blocks the water molecules from directly contacting the oxide passivation layer and phosphorus. Although the first BP layer is still oxidized by O₂, it is isolated from ambient humidity by the hydrophobic alkyl monolayer, which prevents the water from dissolving this top native oxide that would have perpetuated the corrosion. Our experimental finding of the passivation effect on BP is consistent with the theoretical prediction that mere BP + O₂ reaction forming BP-PO_x should be fully stable and self-limiting at ~1 to 2 nm if no moisture exists (31).

In summary, we have developed a strategy to effectively slow down the corrosion of BP by coating of alkylamine monolayer onto its surface. General applicability on a variety of other layered materials is also demonstrated. The alkylamine monolayer is robust in a range of chemical and thermal environments, including ambient air. The facile coating method can be implemented

with many different substrates and is compatible with all linear alkylamines no shorter than *n*-butylamine, thus offering a platform for controlling the surface physics and chemistry of a rich tableau of 2D materials. Because of its simplicity, ecofriendliness, and low cost, we envision it to be scalable and adaptable in various industrial configurations.

ACKNOWLEDGMENTS. C.S. and Z.Y. would like to thank Philip Kim for granting lab access for the glovebox-enclosed AFM. C.S. would like to thank Greg Lin and Frank Zhao for helpful discussions. Z.Y. thanks Pablo Jarillo-Herrero for providing the glovebox. J.L., C.S., M.D. (MIT), and L.S. acknowledge support by the Center for Excitronics, an Energy Frontier Research Center funded by the US Department of Energy, Office of Science, Basic Energy Sciences under Award DE-SC0001088. J.L., C.S., and Z.Y. acknowledge support by NSF ECCS-1610806, the Australian Research Council Discovery Project (Grant DP190100295), and the Australian National University (ANU) Futures Scheme (Grant Q4601024). Q.-B.Y. and G.S. acknowledge support in part by the Ministry of Science and Technology of China (Grant 2013CB933401), the National Science Foundation of China (Grant 11474279), and the Strategic Priority Research Program of the Chinese Academy of Sciences (Grant XDB07010100). H.L. and J.H. acknowledge funding support provided by NSF under Award 1453218. J.H.W. acknowledges the support from the Royal Society. J.K. and C.S. acknowledge support from the US Army Research Office through the Massachusetts Institute of Technology Institute for Soldier Nanotechnologies, under Award 023674. T.Y., N.Z., and K.T. acknowledge support by Inter-University Cooperative Research Program of the Institute for Materials Research, Tohoku University (program no. 15G0031).

1. D. D. Macdonald, Passivity—The key to our metals-based civilization. *Pure Appl. Chem.* **71**, 951–978 (1999).
2. K. F. Mak, C. Lee, J. Hone, J. Shan, T. F. Heinz, Atomically thin MoS₂: A new direct-gap semiconductor. *Phys. Rev. Lett.* **105**, 136805 (2010).
3. H. R. Gutiérrez *et al.*, Extraordinary room-temperature photoluminescence in triangular WS₂ monolayers. *Nano Lett.* **13**, 3447–3454 (2013).
4. Y. Zhang *et al.*, Direct observation of the transition from indirect to direct bandgap in atomically thin epitaxial MoSe₂. *Nat. Nanotechnol.* **9**, 111–115 (2014).
5. J. S. Ross *et al.*, Electrically tunable excitonic light-emitting diodes based on monolayer WSe₂ p-n junctions. *Nat. Nanotechnol.* **9**, 268–272 (2014).
6. X. Qian, J. Liu, L. Fu, J. Li, Quantum spin hall effect in two-dimensional transition metal dichalcogenides. *Science* **346**, 1344–1347 (2013).
7. Y. Yu *et al.*, Gate-tunable phase transitions in thin flakes of 1T-TaS₂. *Nat. Nanotechnol.* **10**, 270–276 (2015).
8. L. Tao *et al.*, Silicene field-effect transistors operating at room temperature. *Nat. Nanotechnol.* **10**, 227–231 (2015).
9. A. Favron *et al.*, Photooxidation and quantum confinement effects in exfoliated black phosphorus. *Nat. Mater.* **14**, 826–832 (2015).
10. L. Li *et al.*, Black phosphorus field-effect transistors. *Nat. Nanotechnol.* **9**, 372–377 (2014).
11. F. Zhu *et al.*, Epitaxial growth of two-dimensional stanene. *Nat. Mater.* **14**, 1020–1025 (2015).
12. P. Vishnoi, U. Gupta, R. Pandey, C. N. R. Rao, Stable functionalized phosphorenes with photocatalytic HER activity. *J. Mater. Chem. A* **7**, 6631–6637 (2019).
13. A. K. Geim, I. V. Grigorieva, Van der Waals heterostructures. *Nature* **499**, 419–425 (2013).
14. J. D. Wood *et al.*, Effective passivation of exfoliated black phosphorus transistors against ambient degradation. *Nano Lett.* **14**, 6964–6970 (2014).
15. S. Ross, A. Sussman, Surface oxidation of molybdenum disulfide. *J. Phys. Chem.*, **59**, 889–892 (1955).
16. Y. Zhang *et al.*, Controlled growth of high-quality monolayer WS₂ layers on sapphire and imaging its grain boundary. *ACS Nano* **7**, 8963–8971 (2013).
17. S. P. Koenig, R. A. Doganov, H. Schmidt, A. H. Castro Neto, B. Özyilmaz, Electric field effect in ultrathin black phosphorus. *Appl. Phys. Lett.* **104**, 103106 (2014).
18. A. Castellanos-Gomez *et al.*, Isolation and characterization of few-layer black phosphorus. *2D Mater.* **1**, 025001 (2014).
19. J. Gao *et al.*, Aging of transition metal dichalcogenide monolayers. *ACS Nano* **10**, 2628–2635 (2016).
20. M. J. Nine, M. A. Cole, D. N. H. Tran, D. Lasic, Graphene: A multipurpose material for protective coatings. *J. Mater. Chem. A* **3**, 12580–12602 (2015).
21. G. H. Lee *et al.*, Highly stable, dual-gated MoS₂ transistors encapsulated by hexagonal boron nitride with gate-controllable contact, resistance, and threshold voltage. *ACS Nano* **9**, 7019–7026 (2015).
22. H. Y. Chang *et al.*, High-performance, highly bendable MoS₂ transistors with high-k dielectrics for flexible low-power systems. *ACS Nano* **7**, 5446–5452 (2013).
23. S. S. Sabri *et al.*, Graphene field effect transistors with parylene gate dielectric. *Appl. Phys. Lett.* **95**, 9–12 (2009).
24. B. Chamlagain *et al.*, Mobility improvement and temperature dependence in MoSe₂ field-effect transistors on parylene-C substrate. *ACS Nano* **8**, 5079–5088 (2014). Correction in: *ACS Nano* **8**, 8710 (2014).
25. Y. Zhao, Q. Zhou, Q. Li, X. Yao, J. Wang, Passivation of black phosphorus via self-assembled organic monolayers by van der Waals epitaxy. *Adv. Mater.* **29**, (2017).
26. C. Mackin *et al.*, Chemiresistive graphene sensors for ammonia detection. *ACS Appl. Mater. Interfaces* **10**, 16169–16176 (2018).
27. D. H. Kang *et al.*, Controllable nondegenerate p-type doping of tungsten diselenide by octadecyltrichlorosilane. *ACS Nano* **9**, 1099–1107 (2015).
28. Z. He *et al.*, Revealing defect-state photoluminescence in monolayer WS₂ by cryogenic laser processing. *ACS Nano* **10**, 5847–5855 (2016).
29. G. Lamour *et al.*, Contact angle measurements using a simplified experimental setup. *J. Chem. Edu.* **87**, 1403–1407 (2010).
30. D. L. Williams *et al.*, Computerised measurement of contact angles. *Galvanotechnik* **101**, 2502–2512 (2010).
31. M. T. Edmonds *et al.*, Creating a stable oxide at the surface of black phosphorus. *ACS Appl. Mater. Interfaces* **7**, 14557–14562 (2015).
32. G. Kresse, J. Furthmüller, Efficient iterative schemes for ab initio total-energy calculations using a plane-wave basis set. *Phys. Rev. B Condens. Matter* **54**, 11169–11186 (1996).
33. J. P. Perdew, K. Burke, M. Ernzerhof, Generalized gradient approximation made simple. *Phys. Rev. Lett.* **77**, 3865–3868 (1996).
34. G. Kresse, From ultrasoft pseudopotentials to the projector augmented-wave method. *Phys. Rev. B* **59**, 1758–1775 (1999).
35. S. Grimme, J. Antony, S. Ehrlich, H. Krieg, A consistent and accurate ab initio parametrization of density functional dispersion correction (DFT-D) for the 94 elements H-Pu. *J. Chem. Phys.* **132**, 154104 (2010).
36. J. D. Pack, H. J. Monkhorst, “Special points for Brillouin-zone integrations”—a reply. *Phys Rev B* **16**, 1748–1749 (1977).
37. W. Tang, E. Sanville, G. Henkelman, A grid-based Bader analysis algorithm without lattice bias. *J. Phys. Condens. Matter* **21**, 084204 (2009).
38. M. Yu, D. R. Trinkle, Accurate and efficient algorithm for Bader charge integration. *J. Chem. Phys.* **134**, 064111 (2011).
39. T. Low, M. Engel, M. Steiner, P. Avouris, Origin of photoresponse in black phosphorus phototransistors. *Phys. Rev. B* **90**, 1–5 (2014).
40. H. Yuan *et al.*, Polarization-sensitive broadband photodetector using a black phosphorus vertical p-n junction. *Nat. Nanotechnol.* **10**, 707–713 (2015).
41. J. M. Bastidas, J. L. Polo, E. Cano, Substitutional inhibition mechanism of mild steel hydrochloric acid corrosion by hexylamine and dodecylamine. *J. Appl. Electrochem.* **30**, 1173–1177 (2000).
42. B. Long *et al.*, Non-covalent functionalization of graphene using self-assembly of alkane-amines. *Adv. Funct. Mater.* **22**, 717–725 (2012).
43. X. Ling, H. Wang, S. Huang, F. Xia, M. S. Dresselhaus, The renaissance of black phosphorus. *Proc. Natl. Acad. Sci. U.S.A.* **112**, 4523–4530 (2015).
44. J. M. Bastidas, J. D. E. Damborenea, A. J. Va, Butyl substituents in *n*-butylamine and their influence on mild steel corrosion inhibition in hydrochloric acid. *J. Appl. Electrochem.* **27**, 345–349 (1997).
45. S. L. Yau, T. P. Moffat, A. J. Bard, Z. Zhang, M. M. Lerner, STM of the (010) surface of orthorhombic phosphorus. *Chem. Phys. Lett.* **198**, 383–388 (1992).